Thin Solid Films 518 (2010) 5188–5194

Contents lists available at ScienceDirect

Thin Solid Films

journal homepage: www.elsevier.com/locate/tsf

Influence of liquid environments on femtosecond laser ablation of silicon

Hewei Liu [a], Feng Chen [a,*], Xianhua Wang [a], Qing Yang [b], Hao Bian [a], Jinhai Si [a], Xun Hou [a]

[a] Key Laboratory for Physical Electronics and Devices of the Ministry of Education & Shaanxi Key Laboratory of Photonic Technology for Information, School of Electronics & Information Engineering, Xi'an Jiaotong University, No. 28, Xianning West Road, Xi'an, 710049, PR China
[b] State Key Laboratory for Manufacturing Systems Engineering Xi'an Jiaotong University, No. 28, Xianning West Road, Xi'an, 710049, PR China

ARTICLE INFO

Article history:
Received 15 August 2009
Received in revised form 16 April 2010
Accepted 20 April 2010
Available online 26 April 2010

Keywords:
Femtosecond laser
Laser ablation
Scanning electron microscopy
Silicon
Liquids
Confocal microscopy

ABSTRACT

Liquid-assisted ablation of solids by femtosecond laser pulses has proved to be an efficient tool for highly precise microfabrication, which evokes numerous research interests in recent years. In this paper, we systematically investigate the interaction of femtosecond laser pulses with silicon wafer in water, alcohol, and as a comparison, in air. After producing a series of multiple-shot craters on a silicon wafer in the three types of environments, surface morphologies and femtosecond laser-induced periodic surface structures are comparatively studied via the scanning electron microscope investigations. Meanwhile, the influence of liquid mediums on ablation threshold fluence and ablation depth is also numerically analyzed. The experimental results indicate that the ablation threshold fluences of silicon are reduced by the presence of liquids (water/alcohol) and ablation depths of craters are deepened in ambient water. Furthermore, smoother surfaces tend to be obtained in alcohol-mediated ablation at smaller shot numbers. Finally, the evolution of the femtosecond laser-induced periodic surface structures in air, water and alcohol is also discussed.

1. Introduction

Femtosecond laser ablation of solid materials in liquid environments evokes extensively research interests due to its numerous advantages and potential applications in microfabrication. Compared to the common dry treatments, the presence of liquids provides a better heat sink, cooling the sample surfaces efficiently and consequently, reducing the laser-induced residual thermal damages. Recently, Li et al. used a femtosecond laser to ablate 6H-SiC assisted by alcohol, which produced a cleaner and better ablation process than in ambient air [1]. Furthermore, the bubbles generated by evaporation of the surrounding liquid layer could remove the ablation debris which would deposit on the sample surface and scatter the incident lasers. Thus, liquid environments were introduced to precise fabrication of microstructures embedded in transparent materials using femtosecond laser pulses [2–5]. In addition, femtosecond laser ablation of solids in liquids was an efficient tool to generate a large variety of metallic nanoparticles and surface nanostructures because of the confinement effects [6–10].

Silicon is one of the most commonly used semiconductors in microelectromechanism system devices and silicon-based optoelectronic devices. The interaction of femtosecond laser with silicon has attracted considerable attentions in the past decades. Femtosecond laser ablation characteristics and microstructures formed on silicon surfaces after femtosecond laser irradiation were widely studied in vacuum and gases [11,12]. Besides, some research groups have concentrated on the liquid-assisted processing of silicon by femtosecond laser pulses. For example, Daminelli et al. investigated femtosecond laser single-pulse interaction of silicon underwater, and demonstrated that the ablation morphological characteristics of the laser-induced craters produced in water and air are different [13]. Similar works have been done by S. Besner et al., they studied the influence of ambient mediums (air, vacuum and water) on femtosecond laser processing of silicon [14]. Moreover, it was reported that submicrometer-sized surface structures, such as spikes and ripples, were induced in ambient water by femtosecond laser irradiations [15,16]. Reviewing previous works, most of them employed water as the processing environment during the femtosecond laser interaction of silicon, and very few of them reported the influences of different liquid environments on femtosecond laser ablation of silicon. Here, we provide insights into the interaction of femtosecond laser with silicon in ambient alcohol and water. It is expected that this work could help for the high-precise microfabrication and laser-matter interactions in liquid mediums.

In this paper, we systematically studied the femtosecond laser ablation of silicon wafer in ambient air, deionized water and alcohol. In the experiments, a series of multiple-shot craters were created by femtosecond laser pulses in these three types of environments. A scanning electron microscope (SEM) and a laser confocal scanning microscope were employed to investigate surface morphologies and measure the size of the craters. Subsequently, ablation threshold fluences and incubation coefficients were evaluated and compared. Finally, we investigated the evolution of femtosecond laser-induced periodic surface structures on silicon as a function of processing environments. It shall be noted that a laser-induced microstructure is

* Corresponding author. Tel./fax: +86 29 82663485.
E-mail address: chenfeng@mail.xjtu.edu.cn (F. Chen).

0040-6090/$ – see front matter © 2010 Elsevier B.V. All rights reserved.
doi:10.1016/j.tsf.2010.04.043

observed in the craters induced in alcohol, and the probable formation mechanisms have been promoted.

2. Experimental details

The sample used in the experiments is a single-crystal silicon (100) wafer. The thickness of the wafer is 400 μm. Before femtosecond laser irradiation, the wafer is cleaned by ultrasonic bath for 15 min in acetone and rinsed in alcohol.

In the experiments, the laser source is a Ti: sapphire oscillator-amplifier system (Femtopower Compact Pro, Femtolasers), which delivered 800 nm, 30 fs Gaussian laser pulses at a repetition rate of 1 kHz. The pulse energy could be continuously varied by a variable attenuator, and a fast shutter was employed to control the pulse number. The laser pulses were focused via a 5× microscope objective (Nikon, NA = 0.15). For liquid experiments, the sample was stuck to the bottom of a 10 ml glass container which is mounted on a computer-controlled three-axis stage (M-505.2DG, Physik Instrumente). When the glass container was filled up with water or alcohol, the thickness of the liquid layer above the sample surface was about 10 mm. Monitoring of the sample was accomplished by a tungsten lamp light source and a CCD camera with a video monitor.

In both air and liquid experiments, all the craters were ablated on an identical silicon wafer. The pulse energies, E_p, used in the experiments were 1.5 μJ, 2.5 μJ, 3.5 μJ and 4.5 μJ. For each energy, craters were produced by different pulse numbers N (N = 10, 100, 500, 1000 and 5000). Considering the different focal conditions in air and liquids due to refractive effects, we adjusted the position of focal plane by moving the sample along the optical axis in order to obtain the same focal positions in the experiments. For air experiments, a series of craters (E_p = 1.5 μJ, N = 1000) were produced on the sample surface under different focal conditions and the focal plane was determined by finding the smallest diameter of the craters. Then we defined this position of focal point as z = 0, where z is the position of z-axis (optical axis). In water and alcohol experiments, the focal planes were determined by the same method. The focal plane for water experiments was found 1.68 mm (z = 1.68) farther than air (z = 0) experiments and 2.03 mm for alcohol experiments (z = 2.03). The increases of focal length were resulted from a larger refractive index of water (1.33) or alcohol (1.38) than air (1.00).

After irradiation, the sample was treated by ultrasonic bath for 5 min both in deionized water and acetone in order to clean the residual ejections of material off the surface. Morphological characteristics were investigated by a scanning electron microscope (JSM-6390, JEOL Ltd., Voltage: 20 kV), diameters and depths of the craters were measured using a laser confocal scanning microscope (VK-9700, KEYENCE Co., Laser source: λ = 408 nm, Objective: N.A. = 0.95).

3. Results and discussion

3.1. Surface morphologies

Fig. 1 shows the SEM images of the craters produced by N = 10, 500 and 5000 at E_p = 2.5 μJ. It apparently indicates that surface morphologies of the craters induced in liquid environments (water/alcohol) are smoother than those produced in ambient air. In air experiments, when the number of incident pulses was relatively small (N = 10), grating-like structures could be found in the whole irradiated regions, as shown in Fig. 1(a). With the increase of pulse number, the surfaces

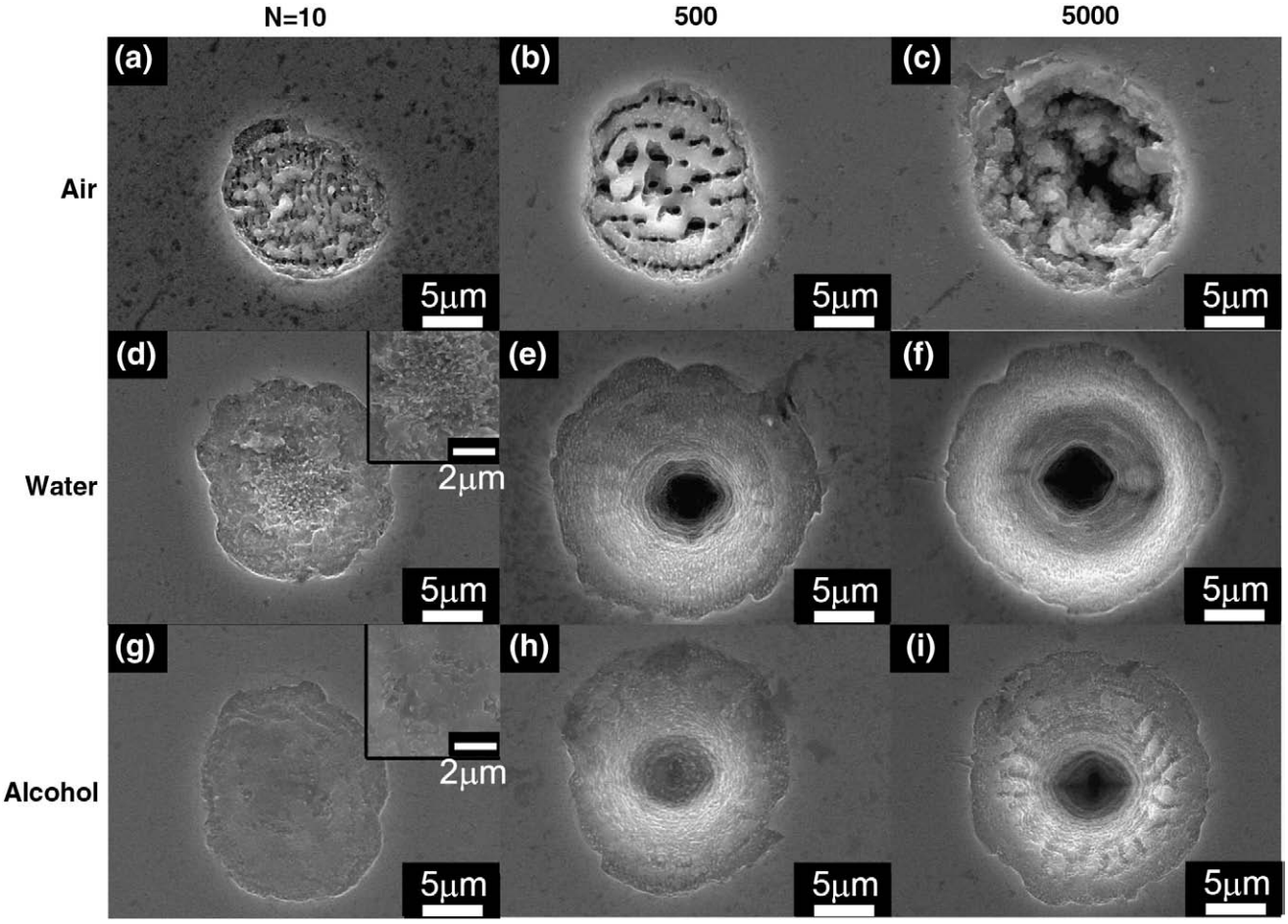

Fig. 1. SEM images of the craters induced in air (a–c), water (d–f) and alcohol (g–i). The pulse energy N_p = 2.5 μJ.

of the irradiated regions became rougher. For example, a porous structure and an unstable loose structure appeared in the 500-shots (Fig. 1(b)) and the 5000-shots crater (Fig. 1(c)). The formation of these structures was associated with various thermal-related processes, including laser-induced melting, surface tension and resolidification of ablated ejections. It demonstrates that thermal effects can be observed in femtosecond laser–silicon interactions at these fluence levels. This is because when the pulse number is large and the pulse energy is relatively high, residual energy and ultrahigh-temperature plasmas will heat the sample surfaces, resulting in the thermal processes, which are so-called residual thermal effects [17,18]. In liquid experiments, as aforementioned, the sample surfaces could be cooled down by the liquids and ejections were also removed by bubbles. Therefore, the thermal effects were not evident and the surface morphologies of the craters became much smoother and cleaner, as shown in Fig. 1(d)–(i). From Fig. 1 we could also observe that for water-mediated ablation, nanometer-sized roughness could be found at smaller shot numbers (Fig. 1(d), $N=10$), which is attributed to the interplay of surface melting and bubble-related mechanical pressures [19,20]. However, the alcohol-mediated ablation tended to obtain smoother and better surfaces than the water-mediated ablation at small pulse numbers, as shown in Fig. 1(g), where $N=10$ and $E_p=2.5$ μJ. The experimental observations via the CCD camera showed that perturbations at the water/silicon interfaces are much more intense than at alcohol/silicon interfaces, which resulted in the formation of the nanoroughness structures of the target ablated in water. For larger numbers of shots, the surfaces of the craters induced in water are smooth and clean (Fig. 1(f), $N=5000$), but radial microroughnesses appeared in alcohol experiments (Fig. 1(i), $N=5000$). The formation of these special surface structures will be discussed in Section 3.3.

3.2. Ablation characteristics

To study the ablation characteristics, we initially measured the size of the craters using the laser confocal scanning microscope. Fig. 2 shows the 2D image and cross-sections of the craters produced in air (Fig. 2(a)), water (Fig. 2(b)) and alcohol (Fig. 2(c)) at $E_p=2.5$ μJ and $N=1000$. The figures clearly show that the interactions of femtosecond laser with silicon in air, water and alcohol lead to the formation of several characteristic morphological regions, such as deep craters, melting ejections and protrusions. In all cases presented in this study, the craters' diameters were measured to the outside of crater rim.

3.2.1. Multiple-shots ablation thresholds

The ablation threshold fluences of the silicon wafer in air, water and alcohol were evaluated by investigating the dependency of the crater sizes (squared diameter, D^2) and irradiation pulse energies. By fitting the data according to the equation [21]

$$D^2 = 2\omega_0^2 \ln\left(\frac{E_p}{E_{th}}\right),$$

where ω_0 is the beam radius at focal plane and E_{th} is the threshold energy. We can obtain $\ln E_{th}$ when $D^2 \to 0$. Fig. 3 shows the corresponding results produced by 5000 shots in air, water and alcohol. The threshold fluences, F_{th}, could be calculated with the equation:

$$F_{th} = \frac{2E_{th}}{\pi\omega_0^2}.$$

For $N=5000$ (Fig. 3), the calculated threshold fluences, F_{th}, were (0.27 ± 0.07) J cm^{-2}, (0.19 ± 0.09) J cm^{-2} and (0.18 ± 0.05) J cm^{-2}, for air, water and alcohol, respectively; and the corresponding evaluated beam radiuses, ω_0, were 11.4 μm, 10.3 μm and 10.1 μm (e^{-2}). The difference of the beam radiuses ω_0 between three types of processing

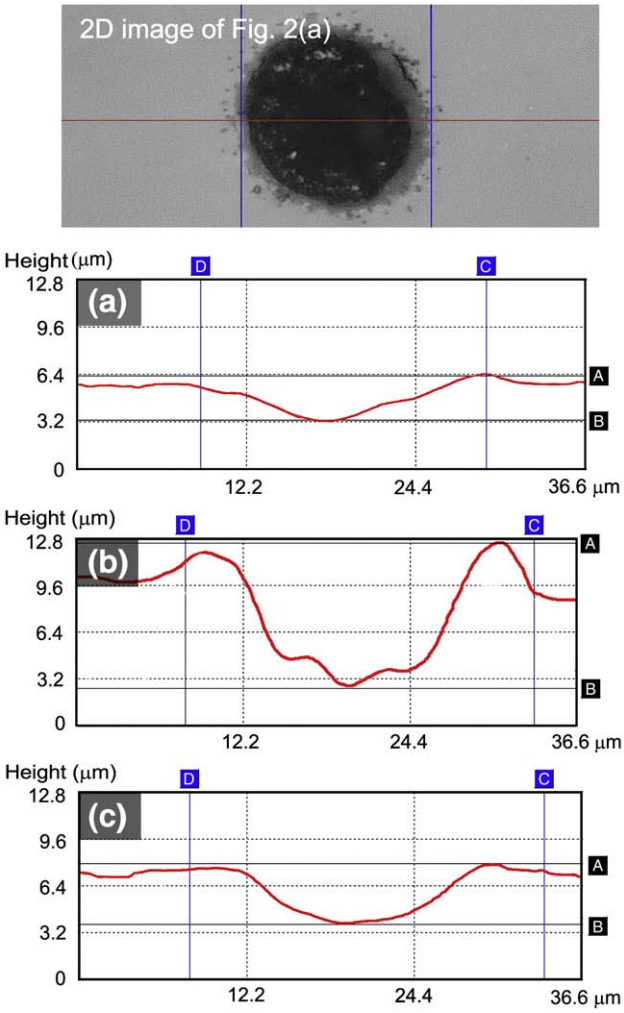

Fig. 2. 2D profiles of the craters produced in air (a), water (b) and alcohol (c). (a) $D=19.2$ μm, $L=2.43$ μm; (b) $D=23.3$ μm, $L=4.11$ μm; (c) $D=22.1$ μm, $L=3.25$ μm.

environments is related to the refractive index effects (the refractive index of air, water and alcohol is 1.00, 1.33 and 1.38, respectively). Other ablation threshold values for $N=10$, 100, 500, 1000 and 5000 were evaluated by the same method and shown in Table 1.

From Table 1, we can see that the ablation threshold fluences F_{th} for air experiments are somewhat higher than those for liquid (water/alcohol) experiments. Take $N=10$ as an example, the F_{th} is (0.44 ± 0.01) J cm^{-2}, (0.37 ± 0.02) J cm^{-2} and (0.38 ± 0.02) J cm^{-2}, for air, water and alcohol, respectively. It should be noted that, the tendency that the ablation threshold fluences for air are higher than those for liquids obtained in our experiments coincides well with the results obtained by Besner et al., who evaluated 10-shot ablation threshold fluence of silicon for air was slightly higher than for water.

The detailed comparison of the threshold fluences for air, water and alcohol is shown in Fig. 4, where $\Delta_1=[F_{th}(\text{air})-F_{th}(\text{water})]/F_{th}(\text{air})\times100\%$ and $\Delta_2=[F_{th}(\text{air})-F_{th}(\text{alcohol})]/F_{th}(\text{air})\times100\%$, denotes the difference of the threshold fluences for air, water and alcohol. The result indicates that the calculated threshold fluences in ambient air are 15%–30% higher than in liquids (water/alcohol) and the difference between air and liquids are enhanced by increasing the number of shots. The enhancement of the ablation threshold fluences in liquids would be related to the different optical properties at the interfaces of transparent mediums and the silicon wafer. In liquid-mediated irradiations, the laser would be reflected at both air/liquids and liquids/silicon interfaces. While in air experiments, the reflection

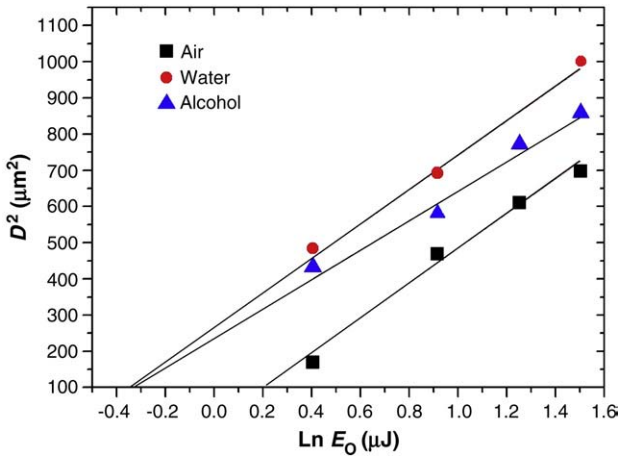

Fig. 3. The dependence of D^2 on lnE_0 as an example for the evaluation of ablation threshold fluences, F_{th}. When $N=5000$, $F_{th}=(0.27\pm0.07)$ J cm^{-2}, (0.19 ± 0.09) J cm^{-2} and (0.18 ± 0.05) J cm^{-2} for air, water and alcohol.

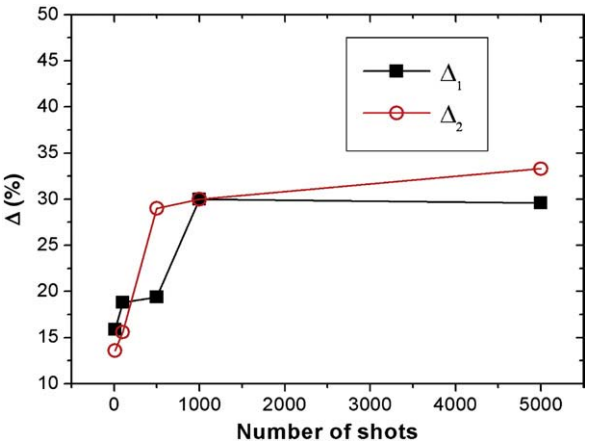

Fig. 4. Comparison of the ablation threshold fluences between air/water (Δ_1) and air/alcohol (Δ_2), where $\Delta_1=[F_{th}\ (\text{air})-F_{th}\ (\text{water})]/F_{th}\ (\text{air})\times100\%$, $\Delta_2=[F_{th}\ (\text{air})-F_{th}\ (\text{alcohol})]/F_{th}\ (\text{air})\times100\%$. More details in text.

only occurs at air/silicon interface. Subsequently, let's evaluate the energy loss caused by the interfacial reflection. The reflection coefficient R for the incident laser at interfaces can be determined by equation:

$$R=\frac{(n-n_0)^2+\kappa^2}{(n+n_0)^2+\kappa^2},$$

where n and κ are the real part and the imaginary part of the refractive index of the target, n_0 is the refractive index of the ambient medium. At air/liquids interfaces, considering $\kappa=0$ for liquids, R is calculated to be 2.0×10^{-2} for the air/water interface and 2.5×10^{-2} for the air/alcohol interface. At medium/silicon interfaces, n and κ for silicon ($\lambda=800$ nm, 300 K) is 3.42 and 0.004, we could obtain the reflection coefficient $R=29.98\times10^{-2}$, 19.36×10^{-2} and 18.06×10^{-2} for air, water and alcohol ambiences, respectively. Therefore, for the same incident laser fluence, the reflection-induced energy loss in ambient air is 9% to 10% higher than water or alcohol ambiences. So to speak, more energy could be injected into the sample surfaces due to the presence of liquids, resulting in the decrease of the ablation threshold fluence. Furthermore, the enhanced recoil pressures of the laser-induced shockwaves and bubble-related mechanical forces under liquid confinements would also cause the extra damage of the sample [22]. It would also reduce the threshold fluences.

In addition, the threshold fluences for air, water and alcohol decrease with the increase of the pulse numbers. Fig. 5 illustrates the thresholds fluences F_{th} plotted logarithmically over the number of shots for the three types of processing environments. It is well known that femtosecond laser ablation of silicon is characterized by incubation and F_{th} decreases with N according to: $F_{th}\ (N)=F_{th}\ (1)\ N^{\xi-1}$, where incubation coefficient ξ is found to be 0.84 or 0.83 for air [13,23] and 0.82 for water [13]. We evaluated the similar $\xi=0.86$, 0.85 and 0.85 for air, water and alcohol, respectively.

Table 1
Ablation threshold fluences, F_{th}, in air, water and alcohol for different numbers of pulses, N.

Number of shots	Ablation threshold fluence(J cm^{-2})		
	F_{th} (Air)	F_{th} (Water)	F_{th} (Alcohol)
10	0.44 ± 0.01	0.37 ± 0.02	0.38 ± 0.02
100	0.32 ± 0.04	0.26 ± 0.01	0.27 ± 0.04
500	0.31 ± 0.06	0.25 ± 0.03	0.22 ± 0.01
1000	0.30 ± 0.07	0.21 ± 0.01	0.21 ± 0.05
5000	0.27 ± 0.07	0.19 ± 0.09	0.18 ± 0.05

3.2.2. Ablation depths

Subsequently, we measured the ablation depth, L, of the laser-induced craters for air, water and alcohol. The dependence of ablation depth L on the number of shots N is presented in Fig. 6. For $E_p=1.5$ μJ and $N<500$, the depths of the craters produced in air are too small to be measured. From the figures, we can see that the ablation depth L of the craters increases sharply with the increase of N and E_p and L complies with the sequence: $L_{water}>L_{alcohol}>L_{air}$. For example, when $E_p=4.5$ μJ and $N=5000$, L was measured as 4.33 μm, 7.03 μm and 6.27 μm for air, water and alcohol. As depicted in Section 3.1, ejections produced by femtosecond laser ablation of silicon deposited inside the irradiated regions and resolidified inside the laser-induced craters, and consequently, the effects of recast decreased the depth of the craters produced by air-mediated ablation, as shown in Fig. 1(c). The presence of liquids could remove the debris and ejections, leading to clean processes and deeper ablation depth. Furthermore, the enhanced mechanical pressures in liquids during femtosecond laser ablation processes would also help to increase the ablation depth [22,24,25].

To explain the difference of the ablation depth between water and alcohol, we considered the energy loss of the incident laser pulses in different liquids. It was reported that laser-induced breakdown of water would result in the energy shielding effects [13,26], leading to the energy loss of the incoming laser pulses. In order to study the difference of the ablation depth between water and alcohol experiments, a simple experiment was carried out to compare the energy

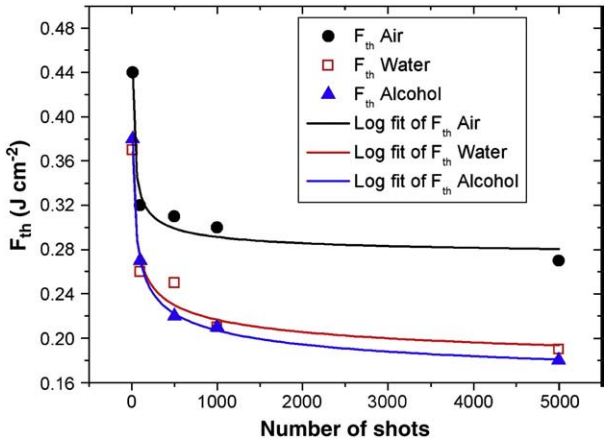

Fig. 5. Logarithmic plot of the ablation threshold fluences vs. shot numbers for the silicon wafer at 30 fs and 800 nm. More details in text.

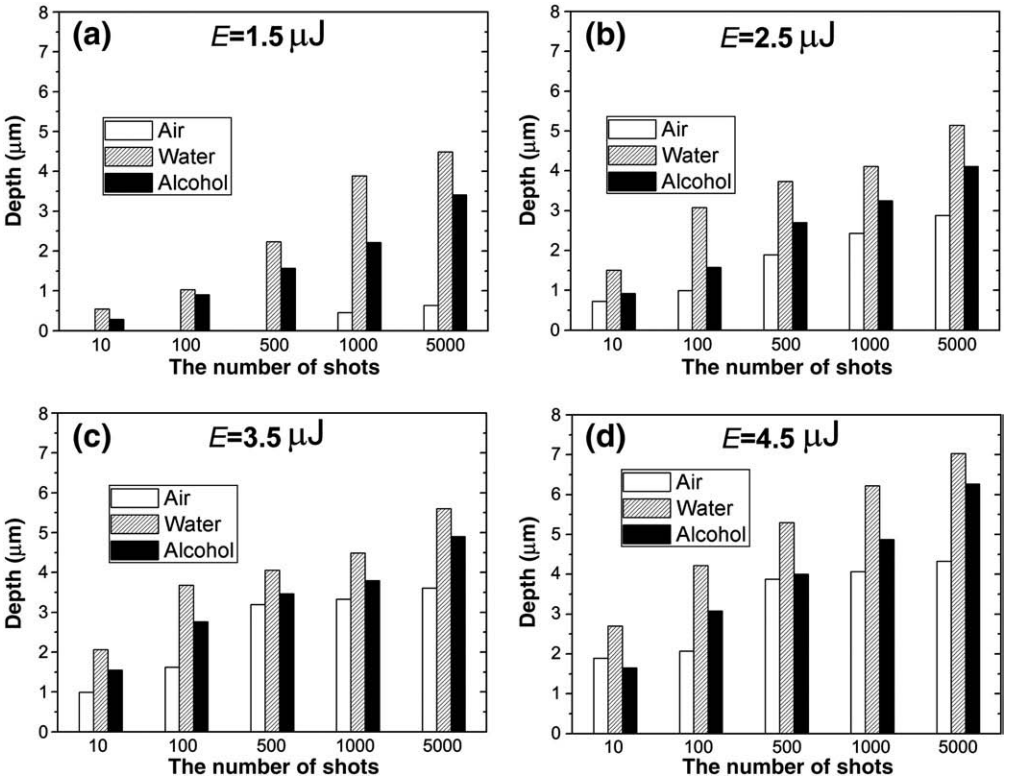

Fig. 6. Comparison of the ablation depths for air, water and alcohol at $E_p = 1.5$ μJ (a), 2.5 μJ (b), 3.5 μJ (c) and 4.5 μJ (d), and the number of shots $N = 10$, 100, 500, 1000 and 5000.

loss induced in water and alcohol. The experimental setup is presented in Fig. 7(a): a lens with focal length of 50 mm was employed to focus the laser pulses (30 fs, 800 nm, 1 kHz) at $E_p = 1$ μJ inside a quartz chamber, which filled up with deionized water or alcohol. Visible supercontinuum lights which are related to the laser-induced breakdown of liquids, were generated and detected by an optical multi-channel analyzer (OMA) placed in optical axis. The result is shown in Fig. 7(b). The supercontinuum lights with spectrum components ranging from 400 nm to 650 nm both for water and alcohol were detected. It shows that the intensity of the supercontinuum generated in alcohol experiment is several times stronger than water. The intensity of the supercontinuum lights will significantly increase upon the appearance of nanoparticles in liquid mediums. Thus, compared to the water, more energy of incoming laser pulses were shielded in the alcohol experiment because of the nanoparticles-related shielding effects, which will reduce the removed materials and ablation depth.

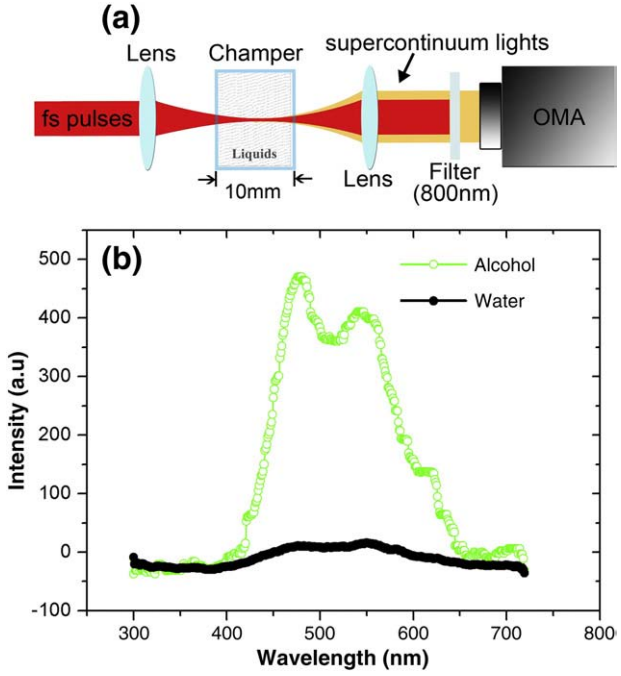

Fig. 7. Measurement of the supercontinuum lights produced by laser-induced breakdown of water and alcohol. (a) Experimental setup. (b) Experimental results. More details in text.

3.3. Femtosecond laser-induced periodic surface structures

In femtosecond laser ablation of solid materials, a universal phenomenon is the appearance of femtosecond laser-induced periodic surface structures, which evokes extensively interests in recent years. Many groups concentrated on the formation mechanisms and applications of these structures. It has been reported that multiple types of structures are observed after femtosecond laser irradiation of metals [27–29], semiconductors [30–32], dielectrics [33–35], and even polymers [36]. Furthermore, it was found that they are dependent on various laser parameters, such pulse energy, pulse number and laser polarization [37]. In our experiments, further SEM studies indicate that liquid environments will affect the femtosecond laser-induced periodic surface structures on silicon. Three different types of structures were found in air, water and alcohol experiments and obtained data are summarized in Table 2.

Fig. 8(a) and (b) shows the first type: grating-like grooves or classic ripples, which are commonly observed after longer-pulsed laser ablation of solids. The grating-like structure, whose period is close to the wavelength of the incident lasers, is resulted from the interference of the incident laser and scattering lights [38]. The similar structures could be also observed in the femtosecond laser ablation of silicon, but the period is 650–750 nm, which is slight smaller

Table 2
Different types of the structures produced on silicon at various conditions.

Processing environments	Pulse energy	Number of shots				
		10	100	500	1000	5000
Air	1.5	☆	☆	☆	×	×
	2.5	☆	☆	×	×	×
	3.5	×	×	×	×	×
	4.5	×	×	×	×	×
Deionized water	1.5	×	×	■	■	■
	2.5	×	×	■	■	■
	3.5	×	×	■	■	■
	4.5	×	×	■	■	■
Alcohol	1.5	×	×	■	△	△
	2.5	×	×	×	■	△
	3.5	×	×	■	■	△
	4.5	×	×	■	■	△

"☆, ■, △": The ability to form wavelength-dependent gratings, nanorods, and radial microgrooves, respectively.
"×": Without ability to form the femtosecond laser-induced periodic surface structures.

than the wavelength of the laser pulses (800 nm). Commonly, the periodicities of such classic ripples were determined by equation [39]: $d = \lambda/(\eta \pm \sin\theta)$ with $\boldsymbol{g}||\boldsymbol{E}$, where λ is the wavelength of incident laser, $\eta = \mathrm{Re}[\varepsilon/(\varepsilon+1)]^{1/2}$ the real part of the effective refractive index of medium-material interface, ε the dielectric constant of the material, θ the laser incidence angle which is 0° in our experiments, $\boldsymbol{g}$ the grating vector, and $\boldsymbol{E}$ is the electrical field of the incident laser. In femtosecond ablation, laser pulses result in dense plasmas, altering the effective refractive index of medium-material interface, η, which is the reason for the shrink of periodicities. In air experiments, such classic ripples appeared only when $N<1000$ and $E_p<3.5$ μJ. For larger pulse numbers and pulse energies, thermal effects dominated the ablation processes, disrupting the formation of periodic surface structures and leading to the appearance of unstable structures, as shown in Fig. 1(b) and (c).

In water experiments, classic ripples were not observed and another type of structure appeared, as shown in Fig. 8(c) and (d). From the figures, we can see that uniform nanorods grow on the walls of the laser-induced craters (Fig. 8(d)). The feature size of these nanorods is 100–140 nm, which are significantly smaller than the wavelength of the incident laser. It is interesting to note that this type of deep-subwavelength structures can only observed at larger pulse numbers ($N \geq 500$), while for smaller pulse numbers, only nanoroughness or smooth surfaces could be found, see, for example in Fig. 1(d) ($N=10$, $E_p=1.5$ μJ, in water) and Fig. 1(g) ($N=10$, $E_p=1.5$ μJ, in alcohol). The nanorods could also be found in water-mediated

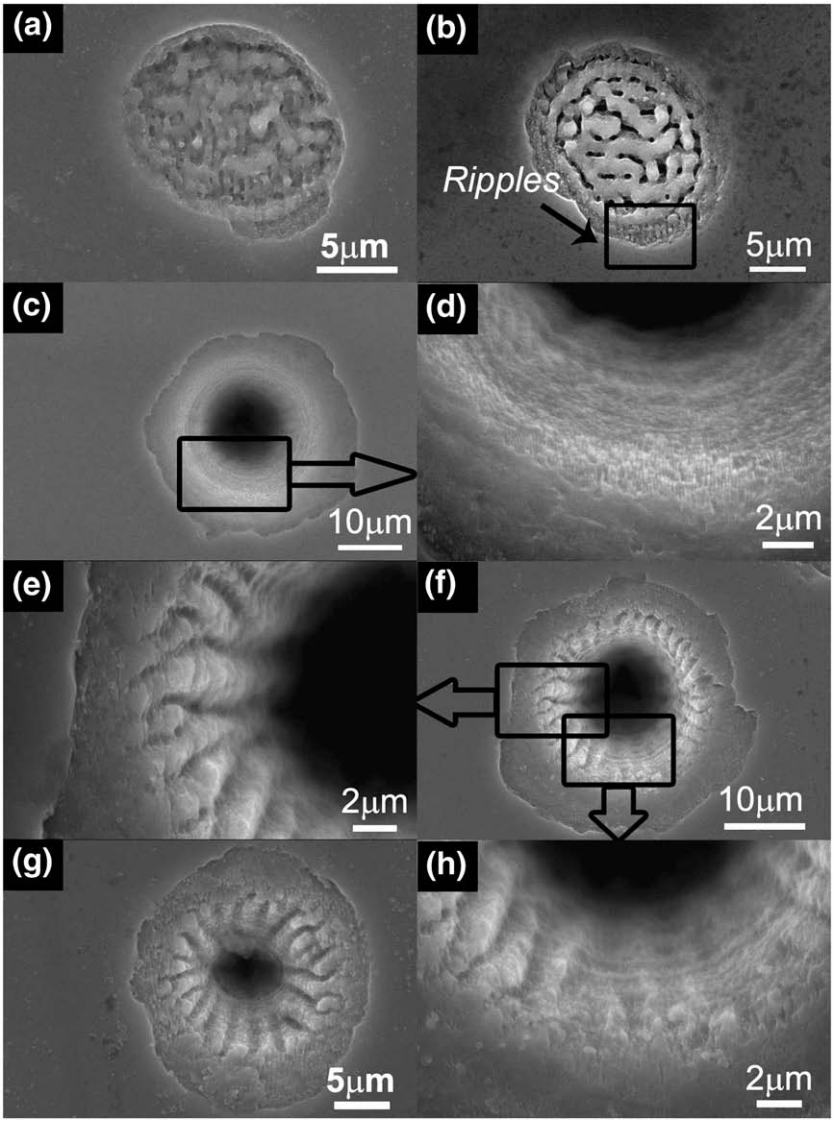

Fig. 8. Femtosecond laser-induced periodic surface structures on the silicon wafer after femtosecond laser irradiations in air (a, b), water (c, d) and alcohol (e–h). (a) $E_p=2.5$ μJ, $N=10$. (b) $E_p=2.5$ μJ, $N=100$. (c, d) $E_p=4.5$ μJ, $N=5000$. (e, f, h) $E_p=4.5$ μJ, $N=5000$. (g) $E_p=3.5$ μJ, $N=5000$.

femtosecond ablation of ZnS and ZnSe [31]. However, the formation mechanism is not clarified. The formation conditions, such as larger pulse number and liquid environments, may demonstrate that it is related to the self-organized process [40]. The interplay of the liquids-related perturbations and surface melting suppressed the formation of classic ripple patterns and the confinement of liquids allowed rapid growth of the nanorods [31].

The nanorods were also observed in alcohol experiments at $N \geq 500$. In addition, we observed radial microgrooves growing on the walls or rims of the craters produced by 500 or 5000-shot irradiations (Fig. 8(e)–(h)). The Fig. 8(e) and (h) show the details of the radial microstructures: the microgrooves, with width of about 1 μm and depth of 1–2 μm, grow on the walls of the craters with the orientation parallel to optical axis, exhibiting radial or daisy-like patterns. The interspacing of the microgrooves is about 2 μm. Microcolumnars reported in Ref. [41] exhibited radial structures, but were dissimilar with the radial microgrooves observed in our experiments. The former structures which were explained by melting–resolidification process and shock-wave effects, spread out of the rim of craters and exceeded the sample surfaces. However, the latter one was more likely photo-etched structures. Gong et al. reported the formation of linear and parallel microgrooves on the walls of craters during femtosecond laser ablation of bulk CdS in water [31]. They employed the interference mechanism to explain the observed microstructures. Although the interspacing of the microgrooves found in their experiments is closed to our results (2–3 μm), but the orientation of the parallel microgrooves was different from the radial microgrooves obtained in our experiments. Further investigations are needed to clarify the formation mechanisms of the radial microgrooves. The interference mechanism may be a suitable interpretation of the formation of such photo-etched periodic microstructures, but still cannot explain the universal occurrence in alcohol environments. In our opinions, complex interactions of the laser, alcohol and silicon, such as laser-induced filaments, mechanical pressures and interference process, probably contribute to the formation of the radial microgrooves.

4. Conclusions

We systematically investigated the femtosecond laser-induced multiple-shots craters on a silicon wafer in ambient air, deionized water and alcohol. The pulse energies E_p used in the experiments are 1.5 μJ, 2.5 μJ, 3.5 μJ and 4.5 μJ, which is higher than femtosecond laser ablation threshold energy of silicon. The number of incident laser pulses $N = 10$, 100, 500, 1000 and 5000. By comparing the surface morphologies, ablation characteristics and femtosecond laser-induced periodic surface structures of the multiple-shot craters, we can obtain following conclusions.

First, the presence of liquids (water/alcohol) could help reducing the thermal damages and removing the ablation debris, and provided cleaner processes during femtosecond laser ablation of silicon wafer than those air-mediated processes. Consequently, the surface morphologies of the craters induced in liquids are much smoother. Furthermore, the surfaces of the craters produced in alcohol are smoother than those induced in water at smaller shot numbers, which might be attributed to the different interacting processes, such as generation of bubbles, recoil pressures and laser-induced surface melting of silicon.

Second, the ablation threshold fluences for air were about 15%–30% higher than for water and alcohol. The threshold fluences for water and alcohol were very close. Decreased reflectivity of the liquid/silicon interfaces for incident laser pulses and enhanced recoil pressures of shockwaves contribute to the shrink of threshold fluences in liquids. Furthermore, the ablation depth of the craters increased with the increase of pulse energy and shots number, and complied with the sequence: $L_{water} > L_{alcohol} > L_{air}$. The liquid cooling effects, bubble-related cleaning effects and shielding effects caused by laser-induced breakdown of liquids were introduced to explain such discrepancy of ablation depth.

Third, three types of surface structures were observed on the surface of the craters induced in air, water and alcohol. In femtosecond laser air-mediated irradiation, we found classic ripples which the interspacing was about 650 nm and close to the wavelength of the incident laser. Nanorods with feature size of 100–140 nm appeared in liquids experiments. In addition, radial-microgroove structures were observed in the alcohol experiments. The dependence of the femtosecond laser-induced periodic surface structures on the pulse energy, shot number and processing environments indicated that the formation of these surface structures may be attributed to various mechanisms, such as interference, self-organization process, mechanical pressures and laser-induced non-linear optical effects in liquids.

Acknowledgements

The authors gratefully acknowledge the financial support for this work provided by the National Science Foundation of China under the Grant Nos. 60678011 and 10674107 and the National High Technology R&D Program of China under the Grant No. 2009AA04Z305.

References

[1] C. Li, X. Shi, J. Si, T. Chen, F. Chen, S. Liang, Z. Wu, X. Hou, Opt. Commun. 282 (2009) 78.
[2] R. An, M.D. Hoffman, M.A. Donoghue, A.J. Hunt, S.C. Jacobson, Opt. Express 16 (2008) 15206.
[3] Y. Li, K. Itoh, W. Watanabe, K. Yamada, D. Kuroda, J. Nishii, Y.Y. Jiang, Opt. Lett. 26 (2001) 1912.
[4] T.N. Kim, K. Campbell, A. Groisman, D. Kleinfeld, C.B. Schaffer, Appl. Phys. Lett. 86 (2005) 201106.
[5] C. Li, X. Shi, J. Si, T. Chen, F. Chen, A. Li, X. Hou, Opt. Commun. 282 (2009) 657.
[6] E. Stratakis, V. Zorba, M. Barberoglou, C. Fotakis, G.A. Shafeev, Appl. Surf. Sci. 255 (2009) 5346.
[7] R.M. Tilaki, A. Irajizad, S.M. Mahdavi, Appl. Phys. A 84 (2006) 215.
[8] E. Stratakis, M. Barberoglou, C. Fotakis, G. Viau, C. Garcia, G.A. Shafeev, Opt. Express 17 (2009) 12650.
[9] A.V. Kabashin, M. Meunier, C. Kingston, J. Luong, J. Phys. Chem. B 107 (2003) 4527.
[10] E. Stratakis, V. Zorba, M. Barberoglou, C. Fotakis, G.A. Shafeev, Appl. Surf. Sci. 255 (2009) 5346.
[11] S. Amoruso, R. Bruzzese, N. Spinelli, R. Velotta, M. Vitiello, X. Wang, G. Ausanio, V. Lannotti, L. Lanotte, Appl. Phys. Lett. 84 (2004) 4502.
[12] T.H. Her, R.J. Finlay, C. Wu, S. Deliwala, E. Mazur, Appl. Phys. Lett. 73 (1998) 1673.
[13] G. Daminelli, J. Krüger, W. Kautek, Thin Solid Films 467 (2004) 334.
[14] S. Besner, J.Y. Degorce, A.V. Kabashin, M. Meunier, Appl. Surf. Sci. 247 (2005) 163.
[15] M.Y. Shen, C.H. Crouch, J.E. Carey, E. Mazur, Appl. Phys. Lett. 85 (2004) 5694.
[16] H. Yonekubo, K. Katayama, T. Sawada, Appl. Phys. A 81 (2005) 843.
[17] A.Y. Vorobyev, C.L. Guo, Appl. Phys. Lett. 86 (2005) 011916.
[18] Y. Hirayama, M. Obara, J. Appl. Phys. 97 (2005) 064903.
[19] G.W. Yang, Progr. Mater. Sci. 52 (2007) 648.
[20] E.V. Zavedeev, A.V. Petrovskaya, A.V. Simakin, G.A. Shafeev, Quant. Electron. 36 (2006) 978.
[21] A. Borowiec, H.F. Tiedje, H.K. Haugen, Appl. Surf. Sci. 243 (2005) 129.
[22] S. Zhu, Y.F. Lu, M.H. Hong, X.Y. Chen, J. Appl. Phys. 89 (2001) 2400.
[23] J. Bonse, S. Baudach, J. Krüger, W. Kautek, M. Lenzner, Appl. Phys. A 74 (2002) 19.
[24] S. Siano, R. Pini, R. Salimbeni, M. Vannini, Appl. Phys. B 62 (1996) 503.
[25] A. Vogel, S. Busch, U. Parlitz, J. Acoust. Soc. Am. 100 (1996) 148.
[26] A. Vogel, J. Noack, K. Nahen, D. Theisen, S. Busch, U. Parlitz, D.X. Hammer, G.D. Noojin, B.A. Rockwell, R. Birngruger, Appl. Phys. B 68 (1999) 271.
[27] A.Y. Vorobyev, V.S. Makin, C.L. Guo, J. Appl. Phys. 101 (2007) 034903.
[28] A.Y. Vorobyev, C.L. Guo, Appl. Phys. Lett. 92 (2008) 041914.
[29] A.M. Kietzig, S.G. Hatzikiriakos, P. Englezos, Langmuir 25 (8) (2009) 4821.
[30] M. Couillard, A. Borowiec, H.K. Haugen, J.S. Preston, E.M. Griswold, G.A. Botton, J. Appl. Phys. 101 (2007) 033519.
[31] W.W. Gong, Z.H. Zheng, J.J. Zheng, H.F. Zhao, X.G. Ren, S.Z. Lu, Appl. Surf. Sci. 255 (2009) 4351.
[32] M.S. Trtica, B.M. Gakovic, B.B. Radak, D. Batani, T. Desai, M. Bussoli, Appl. Surf. Sci. 254 (2007) 1377.
[33] R. Böhme, C. Vass, B. Hopp, K. Zimmer, Nanotechnology 19 (2008) 495301.
[34] M. Shinoda, R.R. Gattass, E. Mazur, J. Appl. Phys. 105 (2009) 053102.
[35] M. Huang, F. Zhao, Y. Cheng, N. Xu, Z. Xu, Opt. Express 16 (2008) 19354.
[36] N. Tsutsumi, A. Fujihara, K. Nagata, Thin Solid Films 517 (2008) 1487.
[37] Q.Z. Zhao, S. Malzer, L.J. Wang, Opt. Lett. 32 (2007) 1932.
[38] Z.G. Sheng, P.M. Fauchet, A.E. Siegman, Phys. Rev. B 26 (1982) 5366.
[39] A.M. Bonch-Bruevich, M.N. Libenson, V.S. Makin, V.V. Trubaev, Opt. Eng. 31 (4) (1992) 718.
[40] F. Costache, M. Henyk, J. Reif, Appl. Surf. Sci. 186 (2002) 352.
[41] T. Matsumura, A. Kazama, T. Yagi, Appl. Phys. A 81 (2005) 1393.